

WildSAT: Learning Satellite Image Representations from Wildlife Observations

Rangel Daroya¹ Elijah Cole² Oisin Mac Aodha³ Grant Van Horn¹ Subhansu Maji¹

¹University of Massachusetts, Amherst ²GenBio AI ³University of Edinburgh

{rdaroya, gvanhorn, smaji}@umass.edu, elijah.cole.cs@gmail.com, oisin.macaodha@ed.ac.uk

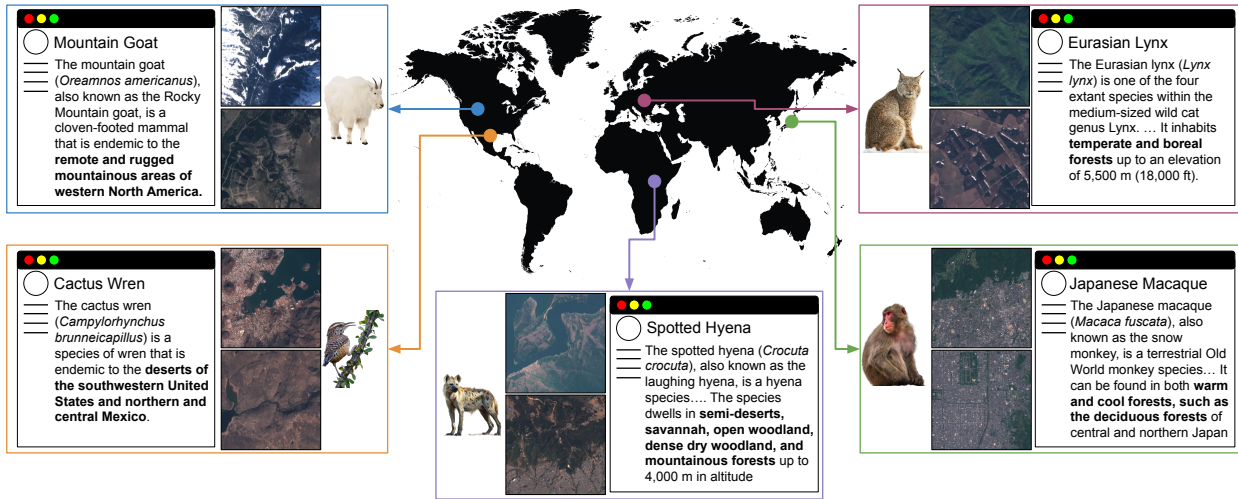


Figure 1. **Wildlife observations can provide valuable supervision for learning satellite image representations.** Known wildlife locations derived from human observations, coupled with descriptive information on species range, habitat, and other ecological attributes on Wikipedia, serve as a rich source of contextual information for satellite imagery. Our **WildSAT** approach leverages these additional data sources to (1) learn satellite image representations, and (2) enable zero-shot satellite image retrieval for identifying species habitats.

Abstract

What does the presence of a species reveal about a geographic location? We posit that habitat, climate, and environmental preferences reflected in species distributions provide a rich source of supervision for learning satellite image representations. We introduce **WildSAT**, which pairs satellite images with millions of geo-tagged wildlife observations readily-available on citizen science platforms. **WildSAT** uses a contrastive learning framework to combine information from species distribution maps with text descriptions that capture habitat and range details, alongside satellite images, to train or fine-tune models. On a range of downstream satellite image recognition tasks, this significantly improves the performance of both randomly initialized models and pre-trained models from sources like ImageNet or specialized satellite image datasets. Additionally, the alignment with text enables zero-shot retrieval, allowing for search based on general descriptions of locations. We demonstrate that **WildSAT** achieves better representations than recent methods that utilize other forms of cross-modal

supervision, such as aligning satellite images with ground images or wildlife photos. Finally, we analyze the impact of various design choices on downstream performance, highlighting the general applicability of our approach.

1. Introduction

The growth in the number of satellites with imaging capabilities deployed over the past 50 years has provided an unprecedented ability to monitor the surface of the earth [36, 75, 77]. The image data derived from these remote sensors has been shown to be highly effective for diverse tasks such as estimating global tree canopy height [38, 65], detecting illegal fishing activity [21, 35, 54], crop monitoring [18, 32, 71], disaster management [55, 63, 69], among others. Central to building computer vision models for these tasks is the need for mechanisms for learning effective representations from image data. As a result of the distribution shift between remote sensing imagery and web-sourced images, a large body of work has emerged exploring the merits and trade-offs between different sources of supervision.

Direct supervision in the form of paired images and labels (*e.g.* image tiles with labels denoting land cover type) can be prohibitively expensive to obtain at a global scale [27]. To address this, there is growing interest to develop methods that learn remote sensing representations from self-supervision [31, 44, 46], multiple paired modalities [14, 45, 60], or other auxiliary sources [15, 68]. For a supervision source to be useful, it needs to be globally distributed, correlated with the local landscape as viewed from an image, and able to discriminate regions at a fine spatial scale.

One promising auxiliary supervision source is provided by the locations where different species of plants and animals can be found around the world. For example, at a coarser scale, *Mountain Goats* (*Oreamnos americanus*) are found in rugged mountainous areas, while at a finer scale, other species such as the *Cactus Wren* (*Campylorhynchus brunneicapillus*), are more habitat specialists as they are typically found in deserts nesting in spiny cacti (Figure 1). This information about where species can be found is an extremely rich source of potential supervision as it characterizes the local natural environment near each observation. It is also readily available online from citizen science platforms such as iNaturalist [2] and eBird [61] which contain hundreds of millions of wildlife location observations. While it has been shown that the locations of species can be used to improve fine-grained species classification [5, 9, 42, 60], it is not clear if this signal is useful for learning informative remote sensing representations.

We introduce a new approach that uses signals derived from species location observations. We take inspiration from recent work that attempt to fuse multi-modal ecological data and remote sensing imagery into a shared common embedding space [28, 59, 60]. Using a contrastive learning objective, WildSAT minimizes the distance between embeddings that describe the same location, utilizing species observation data for combining the different modalities. Feature embeddings of satellite image, text, and location are aligned more closely when they originate from the same area, and moved further apart otherwise. Through this method, we utilize information about the preferred habitats of species to improve satellite image representations.

We make the following contributions: (i) We introduce **WildSAT**, a new approach for learning remote sensing visual representations that exploits the supervision signal provided by the locations where different species have been observed. (ii) We demonstrate zero-shot satellite image retrieval capabilities using text descriptions of habitats and species. (iii) We present a detailed evaluation and show that WildSAT-derived representations outperform, and are complementary to, existing methods on a diverse set of models and downstream remote sensing tasks. (iv) We perform ablation studies to show the relative benefits of each compo-

nent of our approach, and additionally show that WildSAT outperforms recent cross-modal learning approaches such as GRAFT [45] and TaxaBind [60].

2. Related Work

Previous works learn satellite image representations by training on large-scale remote sensing datasets from programs like Landsat [48], Sentinel [17, 29], or NAIP [49]. These methods range from using self-supervised [12, 31, 46], supervised [4, 52, 62], and cross-modal [14, 22, 45, 51, 56, 60] learning to learn rich image representations for downstream satellite-based tasks.

Self-Supervised Learning. These methods learn representations by taking advantage of spatio-temporal invariance or by predicting missing image patches from satellite images. SeCo [46] collects data from the same location across different seasons and uses a contrastive objective to force the image embeddings of samples to be closer if they are from the same location, and farther otherwise. Other works [44, 76] extend this by selecting points in time based on the level of similarity between satellite images, or by synthetically generating images that are variants of the same location. Vision transformers trained using masked autoencoders [12, 26, 31] have also been adopted owing to their success in learning natural image representations. A notable example is Prithvi [31], a transformer network with 100 million parameters pretrained on 1TB of satellite imagery from around the world, achieving strong performance across a variety of Earth observation tasks.

Supervised Learning. These methods leverage labels from tasks like object detection [73], instance segmentation [70], and classification [27, 62] in the satellite domain. Some works focus solely on image classification [52, 62, 70, 72, 73], while others learn from multiple label types. For example, SatlasPretrain [4] curated a large dataset with over 300 million labels across 137 categories, using domain experts, crowdsourced workers, and publicly available datasets (*e.g.* OpenStreetMap [23], WorldCover [66]). It is a unified model trained using multi-tasking across tasks (*e.g.* segmentation, object detection) and showed improved performance on various downstream remote-sensing tasks, significantly outperforming ImageNet-pretrained models and other baselines.

Cross-Modal Learning. Recently, other works have explored adding other modalities while training on satellite images such as Synthetic Aperture Radar (SAR) [22], location [34, 59, 68], text [28, 45], and audio [14, 33, 60]. A common strategy is to use geo-tagged images and pretrained image-text encoders such as CLIP [57]. Additional modalities are then projected to the embedding space of

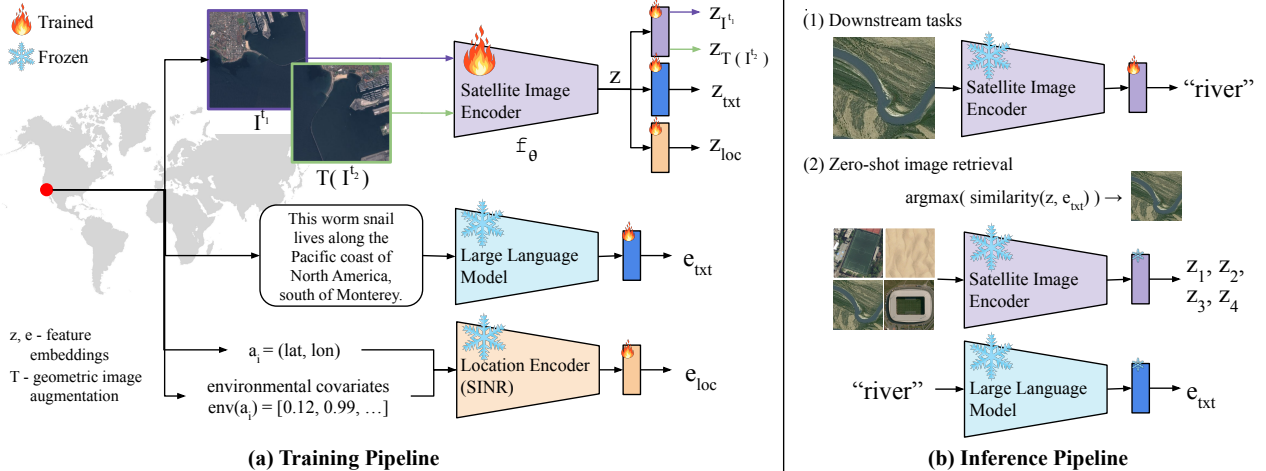


Figure 2. **Architecture for training and evaluating the satellite image encoder.** (a) The training pipeline uses the location of a species, the satellite images at those locations, the environmental covariates, and the Wikipedia text associated with the species. In addition to the alignment of image, text, and location modalities, the encoder is encouraged to learn additional image features by using temporal and geometric image transformations on the input satellite image. (b) Downstream tasks use the frozen satellite image encoder with an additional trainable linear layer. Alternatively, the predicted image embeddings can be used for zero-shot retrieval via text queries.

these existing models using a contrastive learning objective thereby aligning them [14, 30, 34, 45, 68]. Variations of this use the trained model for satellite image localization in GeoCLIP [68], bird species classification and mapping in BirdSAT [59], and improving image representation for plant species in CRISP [28]. Works such as GRAFT [45], TaxaBind [60], and GeoBind [14] align multiple modalities at the same time for cross-modal retrieval such as satellite to audio or ground image retrieval. Others explore methods outside of contrastive learning [15, 64] by employing supervised learning to fuse embeddings of different modalities such as satellite image with location in Sat-SINR [15] or text with location in LE-SINR [24] to predict species range maps, and fusing satellite images with bioclimatic rasters in SatBird [64] for bird species encounter rate prediction.

Similar to those works, we investigate the use of species observation data to learn satellite image representations. Specifically, we explore how habitat preferences, climate, and other environmental factors encoded in species descriptions can serve as supervisory signals. While most previous work has focused on improving species distribution modeling [15, 41, 59, 64] or fine-grained image classification [14, 43, 60] using satellite images, our work improves satellite image representations using wildlife observations. Our experiments show that both randomly initialized models as well as strong baselines, such as Prithvi [31], SatsatNet [4], and SeCo [46], benefit from this supervision on a wide range of satellite image recognition tasks (Table 1).

3. Method

We define the problem as follows: given an image encoder $f_\theta : \mathbf{I} \rightarrow \mathbf{z}$ with parameters θ , we want to find an optimal set

of parameters θ^* that improves the performance of f on various remote sensing tasks through a robust satellite image feature representation \mathbf{z} . It takes an image $\mathbf{I} \in \mathbb{R}^{W \times H \times 3}$ as input and outputs an embedding $\mathbf{z} \in \mathbb{R}^d$. We propose to optimize θ using our WildSAT framework using data consisting of satellite images, locations, environmental covariates, and text. We hypothesize that leveraging known environmental context around each species observation allows for more effective optimization of model parameters (Figure 1).

3.1. WildSAT

To supplement satellite images, we take advantage of additional modalities that naturally align based on the distribution of species throughout the globe. Information on the habitat of species can provide a rich source of supervision for improving satellite image representations, and we describe how to leverage this through our proposed framework WildSAT. Figure 2 shows the overall architecture used to train a satellite image encoder f_θ . The encoder f can be any architecture (e.g. a ResNet50 [25], ViT-B/16 [16], etc.). The initial parameters θ can be randomly initialized, pre-trained on a different domain (e.g. ImageNet [13]), or pre-trained on a related dataset (e.g. SatlapPretrain [4]). The output embedding \mathbf{z} can be used for downstream remote sensing tasks such as classification and zero-shot image retrieval.

WildSAT aims to improve the model by training on additional modalities related to species observation data. To incorporate other modalities, we use pre-trained models, e.g. SINR [11] for location and GritLM [50] for text.

Location encoder. SINR [11] is primarily used for predicting the presence and absence of species at a location. It does this by training on large collections of species observation

data. It takes location $\mathbf{a}_i = (lat, lon) \in \mathbb{R}^2$ and, optionally, the corresponding environmental covariates $\text{env}(\mathbf{a}_i) \in \mathbb{R}^{20}$ to produce a location embedding in \mathbb{R}^{256} .

Large Language Model. GritLM [50] is a large language model (LLM) that outputs a fixed-length embedding in \mathbb{R}^{4096} given a text input. It is trained to handle text of arbitrary length, making it suitable for the varying lengths of text obtained from sources such as Wikipedia [3].

Satellite Image Encoder. Given an initial image encoder f , we add three sets of linear layers to predict embeddings for images (\mathbf{z}_{I^t}), text (\mathbf{z}_{txt}), and locations (\mathbf{z}_{loc}). Similarly, both the pre-trained LLM (GritLM) and location encoder (SINR) have an added trainable linear layer to project their respective feature embeddings to \mathbb{R}^d as \mathbf{e}_{txt} and \mathbf{e}_{loc} , respectively. In addition to text and location, we also fine-tune the model on image-specific features by forcing embeddings of similar satellite images to be close to one another. For two satellite images \mathbf{I}^{t_1} and \mathbf{I}^{t_2} taken at the same location but at different times, their corresponding feature representations should be similar. We also apply geometric augmentations T such as flipping and random cropping on the latter image such that $f(\mathbf{I}^{t_1}) \approx f(T(\mathbf{I}^{t_2}))$. Doing this encourages the model to learn meaningful image features by distinguishing between similar/dissimilar images while refining the same features through the text, location, and environment.

3.2. Dataset

To train the model, we combine images, text, location, and environmental covariates from publicly available datasets [3, 11, 17, 19, 24]. For a given species, we obtain its corresponding observation data through iNaturalist [67], and a text description of its preferred habitat from its corresponding Wikipedia [3] page (Figure 1). Satellite images are then retrieved based on the species observation locations. We describe each component of the dataset below.

Location Observation Data. iNaturalist [67] observations consist of latitude and longitude values denoting the locations where a species has been observed. We use the dataset from SINR [11] that contains 35.5 million observations of 47,375 different species. It is composed of $\{(\mathbf{a}_i, b_i)\}_{i=1}^N$ pairs where $\mathbf{a}_i = (lat, lon)$ is the location and $b_i \in \{s_1, s_2, \dots, s_M\}$ is an integer encoding the species name of the observed species. The locations of each species are used as the basis for matching other sources of data such as environmental covariates, satellite images, and text.

Environmental Covariates. Environmental covariates are obtained from WorldClim2 [19] for a location \mathbf{a}_i . The data aggregates temperature and precipitation values and are often used for ecological applications. It returns a vector for each location $\text{env}(\mathbf{a}_i) \in \mathbb{R}^{20}$. We use five minute resolution data and bilinearly interpolate between data points to get values for specific locations.

Satellite Images. Sentinel-2 satellite images are used with

a resolution of ten meters per pixel, and size 512×512 . The satellite provides 13 spectral bands at different resolutions and has a revisit frequency of five days near the equator. For simplicity and general applicability, since different satellites could sample different sets of bands, we only use RGB bands. We additionally remove satellite images with significant cloud cover. Satellite images taken at the same locations but at a different time are collected as a form of augmentation for training. A total of 305,689 satellite images are collected from EU’s Sentinel data [4, 17].

Text. For each species, we use readily available text data. The text is taken from Wikipedia [3] as in LE-SINR [24]. The corresponding page typically has several sections describing different aspects of the species such as its habitat, range, behavior, taxonomy, *etc.* Each section is processed separately such that one text embedding corresponds to a single section of the Wikipedia text. Similar to [24], we remove sections that do not provide information about the species (*e.g.* references, bibliography, links). The final text dataset contains 127,484 sections from 37,889 species.

For a single satellite image-species location match, there could be multiple text embeddings that correspond to the multiple sections of the species Wikipedia [3] page. Taking these into account, there are a total of 980,376 training samples with location, satellite image, and text. During training, we randomly sample one section of text for every satellite image-species location match, resulting in effectively 134,890 iterations per epoch. We show the spatial distribution of the data in the Appendix.

3.3. Training

Our framework uses a contrastive learning objective to improve the satellite image encoder embeddings. We jointly optimize the parameters of the model f_θ and the additional linear layers through the training objective in Eqn. 1. These loss terms correspond to a contrastive objective over image embeddings (\mathcal{L}_{img}), text embeddings (\mathcal{L}_{txt}), and location embeddings (\mathcal{L}_{loc}) of f , and the overall objective is:

$$\min_{\theta} \left[\underbrace{\mathcal{L}(\mathbf{Z}_{\mathbf{I}^{t_1}}, \mathbf{Z}_{T(\mathbf{I}^{t_2})})}_{\mathcal{L}_{\text{img}}} + \underbrace{\mathcal{L}(\mathbf{Z}_{\text{txt}}, \mathbf{E}_{\text{txt}})}_{\mathcal{L}_{\text{txt}}} + \underbrace{\mathcal{L}(\mathbf{Z}_{\text{loc}}, \mathbf{E}_{\text{loc}})}_{\mathcal{L}_{\text{loc}}} \right] \quad (1)$$

We compute the distance between two sets of embeddings \mathbf{Z} and \mathbf{E} using a minibatch of n samples with the i -th embedding in \mathbf{Z} aligned with the i -th embedding of \mathbf{E} . That is, given two sets of embeddings $\mathbf{Z} = \{\mathbf{z}_1, \dots, \mathbf{z}_n\}$ and $\mathbf{E} = \{\mathbf{e}_1, \dots, \mathbf{e}_n\}$, the embedding \mathbf{z}_i is matched to \mathbf{e}_i against other embeddings $\mathbf{e}_{1, \dots, n}$ using the loss in Eqn. 2.

$$\mathcal{L}(\mathbf{Z}, \mathbf{E}) = \frac{1}{2n} \sum_{i=1}^n (\mathcal{L}_{\text{con}}(\mathbf{z}_i, \mathbf{e}_{1, \dots, n}) + \mathcal{L}_{\text{con}}(\mathbf{e}_i, \mathbf{z}_{1, \dots, n})) \quad (2)$$

Based on the InfoNCE loss [53, 57], Eqn. 3 matches embedding \mathbf{z}_i with the corresponding embedding \mathbf{e}_i by minimizing the distance between them with respect to the other embeddings in \mathbf{E} , with temperature hyperparameter τ .

$$\mathcal{L}_{con}(\mathbf{z}_i, \mathbf{e}_1, \dots, \mathbf{e}_n) = -\log \frac{\exp(\mathbf{z}_i \cdot \mathbf{e}_i / \tau)}{\sum_{j=1}^n \exp(\mathbf{z}_i \cdot \mathbf{e}_j / \tau)} \quad (3)$$

3.4. Implementation Details

During training, we fine-tune all satellite image encoders (and the added linear layers) on the species observation dataset using Eqn. 1. For models pre-trained on out-of-domain datasets (e.g. ImageNet1K [13]), we fine-tune specific layers. In particular, we use scale and shift fine-tuning [20, 39] for ResNet50 models which only tunes the BatchNorm parameters. For transformer models like ViT and Swin [40], we use DoRa [47] on the attention layers. These techniques help in the gradual change of parameters such that the model can learn new information about the new domain (i.e. satellite images) without forgetting features it learned on a different domain (i.e. ImageNet).

For a randomly initialized model or a model pre-trained in the same domain (i.e. satellite images), we fine-tune all parameters. While scale and shift fine-tuning and DoRa also results in performance improvements for randomly initialized and in-domain models, greater improvements are observed with fine-tuning all parameters.

4. Experiments

We evaluate the representations learned by **WildSAT** via linear probing experiments. Starting with different models and different parameter initializations (either random or pre-trained), we evaluate the performance before and after fine-tuning. When probing for each downstream dataset, the trained satellite image encoder is frozen and a randomly initialized linear layer is added (Figure 2b.1). Only the linear layer is trained for every downstream task. We do this to evaluate the impact of the learned image embedding \mathbf{z} .

4.1. Satellite Image Classification

Seven remote sensing classification datasets were used as downstream tasks to evaluate the performance of the image embeddings. We evaluate on UCM [74], AID [72], RESISc45 [7], FMoW [8], EuroSAT [27], So2Sat20k [37, 78], and BigEarthNet20k (BEN20k) [37, 62]. The classes vary from man-made structures (e.g. airplanes, buildings) to land type (e.g. forest, vegetation). One of the seven datasets (BEN20k) is a multi-label classification task, and the rest are single-label tasks. We report accuracy for all datasets, except BEN20k which uses micro F1 score. Each of the datasets is described in the Appendix.

4.2. Bird Species Encounter Rate Prediction

We further evaluate our satellite image representations by predicting species encounter rates. SatBird [64] introduces a benchmark for predicting bird species encounter rates for an area given the satellite image. Encounter rates for a location are given as a vector $\mathbf{r} \in [0, 1]^S$ for S species, where the i -th element is the probability for a visitor to observe species i at that location. Three subsets are defined based on the location and season: (1) USA summer, (2) USA winter, and (3) Kenya. For Kenya, all bird species are considered year-round since migration is negligible. Models are evaluated using top- k accuracy, which takes the top k predicted encounter rates in an area and compares the corresponding species with the ground truth species present in the area. k is the number of actual species observed in an area.

4.3. Base Models

Base models refer to the different pre-trained encoders before we fine-tune with WildSAT. We experiment on seven pre-training methods spanning random initialization, in-domain pre-training, and out-of-domain pre-training. These cover different architectures ResNet50, Swin-T, Swin-B, ViT-B/16, and ViT-L/16 for a total of 18 base models.

ImageNet [13] models are pre-trained with supervision on the updated ImageNet1K V2 dataset [58]. Previous works use V1 of the dataset [13], but we opted for the updated version which improves performance on the ImageNet benchmark by 3-4%. We include results on the ImageNet1K V1 pre-trained models in the Appendix.

MoCov3 [6] models are pre-pretrained using self-supervision with InfoNCE [53] on ImageNet1K.

CLIP [57] uses a contrastive objective to train an image and text encoder on image-text pairs from the Internet.

Prithvi-100M [31] models are pre-trained using self-supervision (MAE [26]) on the Harmonized Landsat Sentinel-2 (HLS) [10] data.

SatCLIP [34] is a self-supervised approach that uses paired location and satellite images from Sentinel-2. While the model has both a location and image encoder, we only use their image encoder for further fine-tuning and evaluation.

SatlasNet [4] models are pre-trained using supervised learning on the SatlasPretrain dataset. The supervision spans a variety of label types ranging from segmentation to object detection and image classification.

SeCo [46] models are self-supervised on time augmented Sentinel-2 satellite images.

TaxaBind [60] uses contrastive learning to learn a common embedding space for multiple modalities including satellite image, ground image, audio, and taxonomic text.

GRAFT [45] uses contrastive learning with the CLIP encoders to align ground images to satellite images and text.

SatMAE [12] is a self-supervised model that uses MAE [26] on temporal multi-spectral satellite imagery.

Encoder	UCM [74]		AID [72]		RESISC45 [7]		FMoW [8]		EuroSAT [27]		So2Sat20k [78]		BEN20k [62]		
	Base	+WS	Base	+WS	Base	+WS	Base	+WS	Base	+WS	Base	+WS	Base	+WS	
	ViT-B/16	ImageNet [13]	93.2	97.5	84.4	88.9	88.2	93.0	43.8	51.4	94.5	97.3	41.8	55.2	52.3
MoCov3 [6]		94.2	95.1	86.0	86.9	89.1	90.3	51.1	52.9	95.9	97.1	47.6	56.6	51.6	57.0
CLIP [57]		94.5	96.3	86.3	88.0	92.1	93.0	51.5	52.8	92.2	97.1	37.6	49.7	47.1	59.1
Prithvi-100M* [31]		49.7	85.5	35.9	71.2	42.6	73.5	19.2	30.5	67.3	93.5	21.5	45.1	33.6	50.6
SatCLIP* [34]		38.2	50.3	37.4	46.4	40.4	46.2	19.0	20.1	74.6	79.4	39.0	43.1	27.0	28.7
Random weights		4.1	75.5	3.8	62.1	1.9	62.4	8.0	26.0	11.1	90.4	5.9	46.8	0.0	51.2
Swin-T	ImageNet [13]	94.0	96.9	87.9	89.0	90.4	91.8	47.6	50.7	96.2	97.3	48.3	51.5	54.1	57.7
	SatlasNet [4]	89.6	91.2	74.3	81.2	80.2	86.5	31.8	44.6	90.8	95.5	36.4	53.1	48.7	56.5
	Random weights	21.0	81.7	19.5	72.0	19.9	74.9	12.1	33.4	59.9	92.7	21.9	45.9	9.8	52.4
ResNet50	ImageNet [13]	94.2	93.6	87.8	86.7	90.5	90.1	47.3	46.0	95.5	96.0	36.1	46.6	55.8	57.5
	MoCov3 [6]	92.0	93.5	83.0	83.3	88.0	87.6	50.2	45.7	93.5	95.1	27.2	42.5	46.6	53.8
	SatlasNet [4]	86.8	90.1	72.5	79.4	81.8	85.4	34.7	42.4	93.5	95.4	33.9	44.8	44.9	56.4
	SeCo [46]	86.1	88.8	74.3	79.6	80.2	86.3	35.9	42.8	89.7	95.5	39.9	46.0	44.3	57.3
	SatCLIP* [34]	69.4	76.2	63.1	71.8	70.2	78.8	36.2	39.9	83.4	92.9	45.4	44.9	42.3	48.2
	Random weights	24.7	79.9	22.3	68.2	24.5	74.7	12.7	36.9	65.2	92.2	5.9	42.3	19.9	51.3
Overall average	68.8	86.1	61.2	77.0	65.3	81.0	33.4	41.1	80.2	93.8	32.6	47.6	38.5	53.1	
Average w/o random	81.8	87.9	72.7	79.4	77.8	83.5	39.0	43.3	88.9	94.3	37.9	48.3	45.7	53.4	

Table 1. **Results of linear probing different models on seven downstream datasets without (Base) and with (+WS) WildSAT fine-tuning.** Accuracy is reported for all datasets except BEN20k that reports micro F1 score. Base refers to the original models specified as the encoder and +WS refers to the same models further trained on the species observation data. Fine-tuning models with species observation show significant improvement over the base models. Both Prithvi-100M and SatCLIP are pre-trained with multispectral images, but for consistency across downstream datasets and models, only RGB bands are used.

	TaxaBind [60]	GRAFT [45]	CLIP [57]	WildSAT (Ours)
Average Performance	59.8%	65.0%	71.6%	76.6%

Table 2. **Average linear probing performance across all seven satellite image classification datasets using models with CLIP ViT-B/16 as the base.** TaxaBind and GRAFT fine-tune CLIP and use additional modalities (*e.g.* text, satellite images, ground images) for cross-modal tasks. We show that fine-tuning CLIP with WildSAT improves performance on both CLIP and other CLIP-based models. We include accuracy per dataset in the Appendix.

Random denotes randomly initialized models.

5. Results and Discussion

5.1. Downstream Classification Performance

Table 1 displays the results on the 7 downstream classification datasets across 15 different models/architectures. The addition of WildSAT improves 98 out of the 105 settings with an overall average improvement ranging from 7.7% to 17.4% across the different datasets (4.3% to 10.4% without the randomly initialized models).

WildSAT improves satellite image representations. The results in Table 1 highlight the performance improvements WildSAT contributes. These improvements may be attributed to our use of diverse supervision—integrating images, text embeddings, and species data at scale. This strat-

egy ultimately helps in downstream classification, particularly for both increasing true positive rates on classes related to habitats (*e.g.* forests, deserts), while reducing false positives on the same types of classes. We show how classes related to wildlife habitats improve performance in the Appendix. Meanwhile, Table 2 provides a comparison of WildSAT (CLIP ViT-B/16 as base) with TaxaBind [60] and GRAFT [45], both of which also fine-tune CLIP ViT-B/16 using cross-modal supervision from ground images. While the latter two methods show improvements on cross-modal tasks, their performance when linear probed on satellite imagery tasks suffers compared to CLIP, indicating a degree of “forgetting” of the representations. In contrast, our method not only outperforms standard CLIP but also achieves the best results overall.

Satellite pre-trained models see a larger boost in performance.

The results demonstrate that training with WildSAT can improve performance by as much as 10% on satellite pre-trained models such as SeCo and SatlasNet. While models pre-trained on ImageNet and MoCov3 also see performance improvements, we see less improvements on the AID, RESISC45, and FMoW datasets. This could be attributed to the three datasets having less categories related to species habitats (*e.g.* storage tank, airport, church). Additionally, since ImageNet and MoCov3 pre-trained models are already performing effectively, there is little room for improvement. WildSAT is trained on a dataset that is

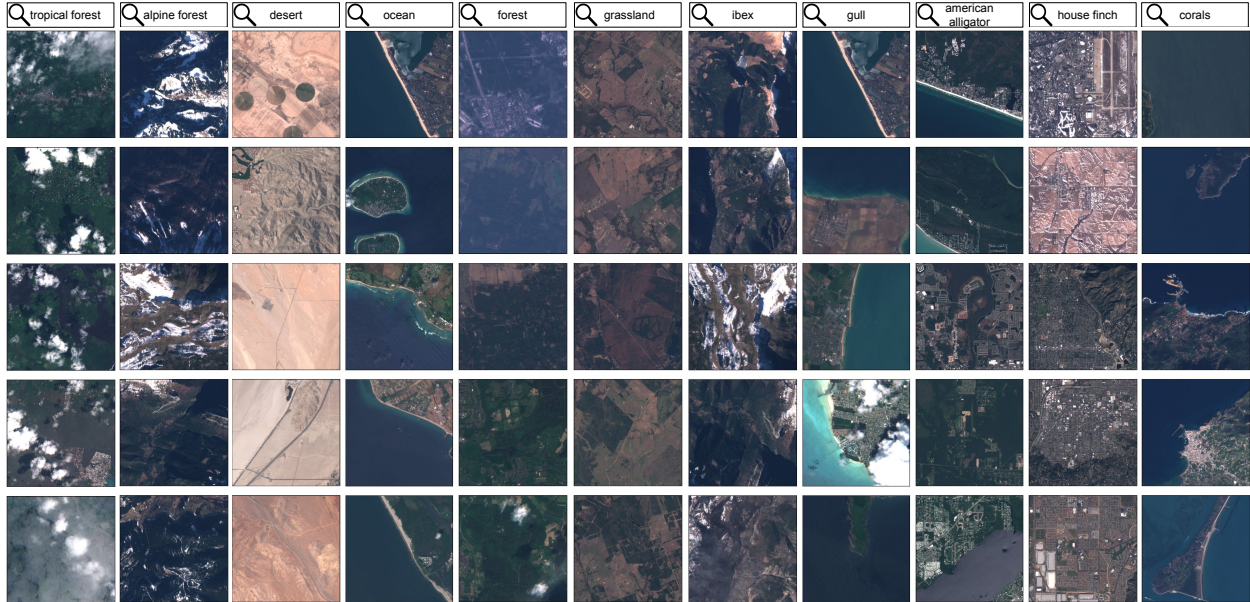


Figure 3. **Zero-shot results for text-based satellite image retrieval.** The columns show the top 5 images returned given the text query on top. A model can be queried using general landscape descriptions such as ‘desert’, ‘ocean’, ‘forest’, and ‘grassland’. In addition, specific wildlife text such as ‘ibex’ and ‘gull’ can be used as queries to view the types of environment they inhabit. The ‘ibex’ inhabits mountains and high elevation areas, ‘gulls’ are typically found near bodies of water, ‘american alligators’ are found in swamps and the coast, the ‘house finch’ is commonly found in urban areas, and ‘corals’ are in the ocean—consistent with the retrieved satellite images shown.

	Kenya		USA Summer		USA Winter	
	Base	+WS	Base	+WS	Base	+WS
SatlasNet [4]	23.90	24.40	48.59	50.03	54.02	55.01
SatMAE [12]	23.66	23.75	46.09	48.69	52.40	53.86
TaxaBind [60]	23.83	24.20	48.31	49.87	53.76	55.00
Average	23.80	24.12	47.66	49.53	53.39	54.62

Table 3. **Top- k accuracy for bird species encounter rate prediction on the SatBird [64] dataset.** Top- k is defined as the accuracy of predicting the k species present in an area.

specifically geared towards habitats and land characteristics. Thus, we see more improvements on So2Sat20k and BEN20k, which cover climate zones and land cover types.

Larger performance gains on ViTs than ResNets. Despite observing smaller improvements with the ResNet50 ImageNet and MoCov3 models, larger improvements are observed with their ViT counterparts. Consistent with observations from previous work [57], we see better performance with the addition of other modalities when using transformers. This could be attributed to the more flexible representations of ViTs, unlike CNNs that inherently incorporate a strong inductive bias from the use of filters. Using attention layers in ViTs likely makes their embeddings more adaptable to other modalities such as text and location.

5.2. Bird Species Encounter Rate Prediction

Table 3 shows WildSAT complementing existing methods on bird species encounter rate prediction. We take models

SatlasNet (Swin-B) [4] and SatMAE (ViT-L/16) [12] presented in SatBird [64] that use satellite images to predict encounter rates of all bird species in an area. TaxaBind [60] is also added as a baseline. Using WildSAT improves these existing methods by 1-2%.

5.3. Zero-shot Image Retrieval

When trained using our WildSAT framework, we observe that models learn wildlife-specific attributes. By using the frozen satellite image encoder and a large language model, a user can input text to query satellite images. The top k images with the most similar embeddings to the text embeddings (computed using cosine similarity) can be retrieved (Figure 2b.2). Figure 3 displays examples of satellite images retrieved given different text queries. General descriptions of landscapes or locations can be used for querying such as ‘desert’, ‘ocean’, ‘forest’, or ‘grassland’. At the same time, specific wildlife text can also be used as queries such as ‘ibex’ or ‘gull’. We see that zero-shot retrieval returns images of the habitat of the corresponding wildlife. This feature could potentially be used to find habitats for species with limited observation data, and can serve as a reference for species distribution studies.

5.4. Ablations

Our WildSAT framework is composed of multiple components: a satellite image encoder, location encoder, and text encoder. We investigate the contribution of each of these components in an ablation study. In Table 4 we ablate two

loc	env	text	img-a	UCM [74]		AID [72]		RESISC45 [7]		So2Sat20k [78]		Average
				Random	ImageNet	Random	ImageNet	Random	ImageNet	Random	ImageNet	
				ResNet50	ViT-B/16	ResNet50	ViT-B/16	ResNet50	ViT-B/16	ResNet50	ViT-B/16	
				24.3%	93.2%	25.2%	84.4%	25.5%	88.2%	5.9%	41.8%	48.6%
✓				44.2%	95.0%	41.6%	85.1%	43.0%	89.3%	18.3%	43.4%	57.5%
✓	✓			60.0%	95.0%	48.7%	86.2%	48.2%	88.8%	25.2%	44.2%	62.0%
✓	✓	✓		70.0%	95.4%	55.6%	86.2%	58.9%	89.7%	27.9%	45.0%	66.1%
✓	✓	✓	✓	79.9%	97.2%	68.2%	88.9%	74.7%	93.0%	42.3%	55.2%	74.9%

Table 4. **Ablation of various components of WildSAT.** The best performance is a combination of all components: location (loc), environmental covariates (env), text (text), and satellite image augmentations (img-a). Results are presented for a randomly initialized ResNet50 model and an ImageNet pre-trained ViT-B/16 model with the numbers referring to linear probing accuracy.

models: a randomly initialized ResNet50 and an ImageNet pre-trained ViT-B/16. Columns with check marks on ‘loc’ and/or ‘env’ indicate the use of the location encoder (\mathcal{L}_{loc} term in Eqn. 1). The location encoder can either use only location as input or use both location and environmental covariates. The ‘text’ and ‘img-a’ columns indicate the use of the large language model (\mathcal{L}_{txt}) and contrastive loss on the augmented satellite images (\mathcal{L}_{img}), respectively. A complete ablation of all possible combinations of WildSAT components for other models is also provided in the Appendix.

Each modality enhances performance. Larger improvements are observed for the randomly initialized model, since it starts from a lower accuracy and there is a larger room for improvement. Nonetheless, similar improvement trends are seen with both types of models. Improvements from location and environmental covariates can be from associating satellite images with particular locations and corresponding environmental characteristics (*i.e.* satellite images are mapped to specific latitudes and longitudes that are along the coast, or in the mountains). The addition of text further improves the performance while enabling zero-shot image retrieval capabilities. Text provides a rich source of information with more detailed descriptions of areas. Adding the satellite image loss term likely improves general image understanding, such as the model learning the rotation invariance of satellite images. Overall, each component of WildSAT contributes to performance improvements.

Different modalities can strengthen models by covering model-specific gaps. We hypothesize that models trained on satellite imagery datasets benefit primarily from location and text supervision associated with wildlife observation. This hypothesis is supported by observations that self-supervised models such as SeCo, SatMAE, and Prithvi—trained with objectives similar to WildSAT’s image self-supervision term on satellite datasets—still achieve significant gains (Table 1). Similarly, models like SatlasNet, which are trained with large-scale supervised learning on satellite images, also benefit. On the other hand, ImageNet pre-trained models benefit from the additional satellite image supervision. These results highlight the complementary nature of WildSAT’s supervision compared to existing

datasets, which primarily focus on anthropogenic labels.

5.5. Limitations

While we show that WildSAT improves satellite image representations and has promising zero-shot performance, the datasets we train on contain inherent limitations that could affect model use. The US and Europe are overrepresented in the data as most citizen contributed data currently come from these locations. Underrepresented areas in Asia, Africa, Australia, and South America are likely to see less accurate results especially on satellite image retrieval. Satellite images additionally do not cover the extreme north and south of the Earth including Antarctica, so species endemic in those areas and their habitats might not be well-represented. We also note that observations of endangered wildlife were excluded or significant noise was added to their locations to ensure their safety. LLMs are further prone to generating hallucinations, which could impact model output reliability.

6. Conclusion

While satellite images are often used to interpolate sparse wildlife observations to create species range maps, our work demonstrates that these observations also provide a rich source of supervision for learning satellite image representations. WildSAT can not only learn high-quality representations from scratch but also improve performance of strong pre-trained models, such as those trained on ImageNet and satellite imagery datasets, across a range of satellite imagery tasks. We attribute this success to the global scale of community efforts, which document diverse wildlife observations through platforms like iNaturalist and eBird and record detailed species attributes on sources like Wikipedia. This supervisory signal complements existing satellite datasets, which often focus on anthropogenic labels, by introducing a broader ecological perspective. As these resources continue to expand in both observational scale (*e.g.* geographical and taxonomic scope) and modality (*e.g.* incorporating sound, aerial imagery), they offer even greater potential for improving WildSAT’s representations.

Acknowledgements. We thank the iNaturalist community for providing the data used for training. Experiments were performed on the University of Massachusetts GPU cluster funded by the Mass. Technology Collaborative. RD and SM were supported in part by NASA grant 80NSSC22K1487 and NSF grant 2329927.

References

- [1] eBird. <https://www.ebird.org>. Accessed on 2024-11-14. 13
- [2] iNaturalist. <https://www.inaturalist.org>. Accessed on 2024-11-14. 2, 13
- [3] Wikipedia. <https://www.wikipedia.org>. Accessed on 2024-11-14. 4, 13
- [4] Favyen Bastani, Piper Wolters, Ritwik Gupta, Joe Ferdinando, and Aniruddha Kembhavi. Satlaspretrain: A large-scale dataset for remote sensing image understanding. In *Proceedings of the IEEE/CVF International Conference on Computer Vision*, pages 16772–16782, 2023. 2, 3, 4, 5, 6, 7, 13, 17
- [5] Thomas Berg, Jiongxin Liu, Seung Woo Lee, Michelle L Alexander, David W Jacobs, and Peter N Belhumeur. Birdsnap: Large-scale fine-grained visual categorization of birds. In *Proceedings of the IEEE conference on computer vision and pattern recognition*, 2014. 2
- [6] Xinlei Chen, Saining Xie, and Kaiming He. An empirical study of training self-supervised vision transformers. In *Proceedings of the IEEE/CVF international conference on computer vision*, pages 9640–9649, 2021. 5, 6
- [7] Gong Cheng, Junwei Han, and Xiaoqiang Lu. Remote sensing image scene classification: Benchmark and state of the art. *Proceedings of the IEEE*, 105(10):1865–1883, 2017. 5, 6, 8, 13, 14, 16, 17
- [8] Gordon Christie, Neil Fendley, James Wilson, and Ryan Mukherjee. Functional map of the world. In *Proceedings of the IEEE Conference on Computer Vision and Pattern Recognition*, pages 6172–6180, 2018. 5, 6, 13, 14, 17
- [9] Grace Chu, Brian Potetz, Weijun Wang, Andrew Howard, Yang Song, Fernando Brucher, Thomas Leung, and Hartwig Adam. Geo-aware networks for fine-grained recognition. In *Proceedings of the IEEE/CVF International Conference on Computer Vision Workshops*, 2019. 2
- [10] Martin Claverie, Junchang Ju, Jeffrey G Masek, Jennifer L Dungan, Eric F Vermote, Jean-Claude Roger, Sergii V Skakun, and Christopher Justice. The harmonized landsat and sentinel-2 surface reflectance data set. *Remote sensing of environment*, 219:145–161, 2018. 5
- [11] Elijah Cole, Grant Van Horn, Christian Lange, Alexander Shepard, Patrick Leary, Pietro Perona, Scott Loarie, and Oisín Mac Aodha. Spatial implicit neural representations for global-scale species mapping. In *International Conference on Machine Learning*, pages 6320–6342. PMLR, 2023. 3, 4, 15, 16
- [12] Yezhen Cong, Samar Khanna, Chenlin Meng, Patrick Liu, Erik Rozi, Yutong He, Marshall Burke, David Lobell, and Stefano Ermon. Satmae: Pre-training transformers for temporal and multi-spectral satellite imagery. *Advances in Neural Information Processing Systems*, 35:197–211, 2022. 2, 5, 7, 14
- [13] Jia Deng, Wei Dong, Richard Socher, Li-Jia Li, Kai Li, and Li Fei-Fei. Imagenet: A large-scale hierarchical image database. In *2009 IEEE conference on computer vision and pattern recognition*, pages 248–255. Ieee, 2009. 3, 5, 6, 14, 15, 16
- [14] Aayush Dhakal, Subash Khanal, Srikumar Sastry, Adeel Ahmad, and Nathan Jacobs. Geobind: Binding text, image, and audio through satellite images. In *International Geoscience and Remote Sensing Symposium*, 2024. 2, 3
- [15] Johannes Dollinger, Philipp Brun, Vivien Sainte Fare Garnot, and Jan Dirk Wegner. Sat-sinr: High-resolution species distribution models through satellite imagery. *ISPRS Annals of the Photogrammetry, Remote Sensing and Spatial Information Sciences*, 2024. 2, 3
- [16] Alexey Dosovitskiy, Lucas Beyer, Alexander Kolesnikov, Dirk Weissenborn, Xiaohua Zhai, Thomas Unterthiner, Mostafa Dehghani, Matthias Minderer, Georg Heigold, Sylvain Gelly, et al. An image is worth 16x16 words: Transformers for image recognition at scale. In *International Conference on Learning Representations*, 2020. 3
- [17] ESA. Sentinel-1-missions-sentinel online-sentinel online. *Eur. Sp. Agency*, 2022. 2, 4, 13
- [18] Joshua Fan, Junwen Bai, Zhiyun Li, Ariel Ortiz-Bobea, and Carla P Gomes. A gnn-rnn approach for harnessing geospatial and temporal information: application to crop yield prediction. In *Proceedings of the AAAI conference on artificial intelligence*, pages 11873–11881, 2022. 1
- [19] Stephen E Fick and Robert J Hijmans. Worldclim 2: new 1-km spatial resolution climate surfaces for global land areas. *International journal of climatology*, 37(12):4302–4315, 2017. 4
- [20] Jonathan Frankle, David J Schwab, and Ari S Morcos. Training batchnorm and only batchnorm: On the expressive power of random features in cnns. In *International Conference on Learning Representations*, 2021. 5, 17
- [21] Rollan C Geronimo, Erik C Franklin, Russell E Brainard, Christopher D Elvidge, Mudjekeewis D Santos, Roberto Venegas, and Camilo Mora. Mapping fishing activities and suitable fishing grounds using nighttime satellite images and maximum entropy modelling. *Remote Sensing*, 10(10):1604, 2018. 1
- [22] Xin Guo, Jiangwei Lao, Bo Dang, Yingying Zhang, Lei Yu, Lixiang Ru, Liheng Zhong, Ziyuan Huang, Kang Wu, Dingxiang Hu, Huimei He, Jian Wang, Jingdong Chen, Ming Yang, Yongjun Zhang, and Yansheng Li. Skysense: A multimodal remote sensing foundation model towards universal interpretation for earth observation imagery. In *Proceedings of the IEEE/CVF Conference on Computer Vision and Pattern Recognition (CVPR)*, pages 27672–27683, 2024. 2
- [23] Mordechai Haklay and Patrick Weber. Openstreetmap: User-generated street maps. *IEEE Pervasive computing*, 7(4):12–18, 2008. 2
- [24] Max Hamilton, Christian Lange, Elijah Cole, Alexander Shepard, Samuel Heinrich, Oisín Mac Aodha, Grant

- Van Horn, and Subhansu Maji. Combining observational data and language for species range estimation. In *Advances in Neural Information Processing Systems*, 2024. 3, 4
- [25] Kaiming He, Xiangyu Zhang, Shaoqing Ren, and Jian Sun. Deep residual learning for image recognition. In *Proceedings of the IEEE conference on computer vision and pattern recognition*, pages 770–778, 2016. 3
- [26] Kaiming He, Xinlei Chen, Saining Xie, Yanghao Li, Piotr Dollár, and Ross Girshick. Masked autoencoders are scalable vision learners. In *Proceedings of the IEEE/CVF conference on computer vision and pattern recognition*, pages 16000–16009, 2022. 2, 5
- [27] Patrick Helber, Benjamin Bischke, Andreas Dengel, and Damian Borth. Eurosat: A novel dataset and deep learning benchmark for land use and land cover classification. *IEEE Journal of Selected Topics in Applied Earth Observations and Remote Sensing*, 12(7):2217–2226, 2019. 2, 5, 6, 13, 14, 17
- [28] Andy V Huynh, Lauren E Gillespie, Jael Lopez-Saucedo, Claire Tang, Rohan Sikand, and Moisés Expósito-Alonso. Contrastive ground-level image and remote sensing pre-training improves representation learning for natural world imagery. In *European Conference on Computer Vision*, 2024. 2, 3
- [29] Markus Immitzer, Francesco Vuolo, and Clement Atzberger. First experience with sentinel-2 data for crop and tree species classifications in central europe. *Remote sensing*, 8(3):166, 2016. 2
- [30] Pallavi Jain, Diego Marcos, Dino Ienco, Roberto Interdonato, Aayush Dhakal, Nathan Jacobs, and Tristan Berchoux. Aligning geo-tagged clip representations and satellite imagery for few-shot land use classification. In *IGARSS 2024-2024 IEEE International Geoscience and Remote Sensing Symposium*, pages 319–323. IEEE, 2024. 3
- [31] Johannes Jakubik, S Roy, CE Phillips, P Fraccaro, D Godwin, B Zadrozny, D Szwarcman, C Gomes, G Nyirjesy, B Edwards, et al. Foundation models for generalist geospatial artificial intelligence, 2023. URL <https://arxiv.org/abs/2310.18660>, 2023. 2, 3, 5, 6, 14
- [32] Priyabrata Karmakar, Shyh Wei Teng, Manzur Murshed, Shaoning Pang, Yanyu Li, and Hao Lin. Crop monitoring by multimodal remote sensing: A review. *Remote Sensing Applications: Society and Environment*, 33:101093, 2024. 1
- [33] Subash Khanal, Srikumar Sastry, Aayush Dhakal, and Nathan Jacobs. Learning tri-modal embeddings for zero-shot soundscape mapping. In *BMVC*, 2023. 2
- [34] Konstantin Klemmer, Esther Rolf, Caleb Robinson, Lester Mackey, and Marc Rußwurm. Satclip: Global, general-purpose location embeddings with satellite imagery. *arXiv preprint arXiv:2311.17179*, 2023. 2, 3, 5, 6, 14, 15, 16
- [35] Andrey A Kurekin, Benjamin R Loveday, Oliver Clements, Graham D Quartly, Peter I Miller, George Wiafe, and Kwame Adu Agyekum. Operational monitoring of illegal fishing in ghana through exploitation of satellite earth observation and ais data. *Remote Sensing*, 11(3):293, 2019. 1
- [36] Nataliia Kussul, Mykola Lavreniuk, Sergii Skakun, and Andrii Shelestov. Deep learning classification of land cover and crop types using remote sensing data. *IEEE Geoscience and Remote Sensing Letters*, 14(5):778–782, 2017. 1
- [37] Alexandre Lacoste, Nils Lehmann, Pau Rodriguez, Evan Sherwin, Hannah Kerner, Björn Lütjens, Jeremy Irvin, David Dao, Hamed Alemohammad, Alexandre Drouin, et al. Geobench: Toward foundation models for earth monitoring. *Advances in Neural Information Processing Systems*, 36, 2023. 5, 13, 15
- [38] Nico Lang, Walter Jetz, Konrad Schindler, and Jan Dirk Wegner. A high-resolution canopy height model of the earth. *Nature Ecology & Evolution*, 2023. 1
- [39] Dongze Lian, Daquan Zhou, Jiashi Feng, and Xinchao Wang. Scaling & shifting your features: A new baseline for efficient model tuning. *Advances in Neural Information Processing Systems*, 35:109–123, 2022. 5, 17
- [40] Ze Liu, Yutong Lin, Yue Cao, Han Hu, Yixuan Wei, Zheng Zhang, Stephen Lin, and Baining Guo. Swin transformer: Hierarchical vision transformer using shifted windows. In *Proceedings of the IEEE/CVF international conference on computer vision*, 2021. 5
- [41] Titouan Lorieul, Elijah Cole, Benjamin Deneu, Maximilien Servajean, Pierre Bonnet, and Alexis Joly. Overview of geolifeclef 2022: Predicting species presence from multi-modal remote sensing, bioclimatic and pedologic data. In *CLEF (Working Notes)*, pages 1940–1956, 2022. 3
- [42] Oisín Mac Aodha, Elijah Cole, and Pietro Perona. Presence-only geographical priors for fine-grained image classification. In *Proceedings of the IEEE/CVF International Conference on Computer Vision*, 2019. 2
- [43] Gengchen Mai, Ni Lao, Yutong He, Jiaming Song, and Stefano Ermon. Csp: Self-supervised contrastive spatial pre-training for geospatial-visual representations. In *International Conference on Machine Learning*, pages 23498–23515. PMLR, 2023. 3
- [44] Utkarsh Mall, Bharath Hariharan, and Kavita Bala. Change-aware sampling and contrastive learning for satellite images. In *Proceedings of the IEEE/CVF Conference on Computer Vision and Pattern Recognition*, pages 5261–5270, 2023. 2, 14
- [45] Utkarsh Mall, Cheng Perng Phoo, Meilin Kelsey Liu, Carl Vondrick, Bharath Hariharan, and Kavita Bala. Remote sensing vision-language foundation models without annotations via ground remote alignment. In *The Twelfth International Conference on Learning Representations*, 2024. 2, 3, 5, 6, 14
- [46] Oscar Manas, Alexandre Lacoste, Xavier Giró-i Nieto, David Vazquez, and Pau Rodriguez. Seasonal contrast: Un-supervised pre-training from uncurated remote sensing data. In *Proceedings of the IEEE/CVF International Conference on Computer Vision*, pages 9414–9423, 2021. 2, 3, 5, 6, 14, 15, 16, 17
- [47] Yulong Mao, Kaiyu Huang, Changhao Guan, Ganglin Bao, Fengran Mo, and Jinan Xu. Dora: Enhancing parameter-efficient fine-tuning with dynamic rank distribution. *arXiv preprint arXiv:2405.17357*, 2024. 5, 17
- [48] Jeffrey G Masek, Michael A Wulder, Brian Markham, Joel McCorkel, Christopher J Crawford, James Storey, and Del T

- Jenstrom. Landsat 9: Empowering open science and applications through continuity. *Remote Sensing of Environment*, 248:111968, 2020. 2
- [49] Aaron E Maxwell, Timothy A Warner, Brian C Vanderbilt, and Christopher A Ramezan. Land cover classification and feature extraction from national agriculture imagery program (naip) orthoimagery: A review. *Photogrammetric Engineering & Remote Sensing*, 83(11):737–747, 2017. 2
- [50] Niklas Muennighoff, SU Hongjin, Liang Wang, Nan Yang, Furu Wei, Tao Yu, Amanpreet Singh, and Douwe Kiela. Generative representational instruction tuning. In *ICLR 2024 Workshop: How Far Are We From AGI*, 2024. 3, 4
- [51] Vishal Nedungadi, Ankit Kariryaa, Stefan Oehmcke, Serge Belongie, Christian Igel, and Nico Lang. Mmearth: Exploring multi-modal pretext tasks for geospatial representation learning. In *European Conference on Computer Vision*, 2024. 2
- [52] Maxim Neumann, Andre Susano Pinto, Xiaohua Zhai, and Neil Houlsby. In-domain representation learning for remote sensing. *arXiv preprint arXiv:1911.06721*, 2019. 2
- [53] Aaron van den Oord, Yazhe Li, and Oriol Vinyals. Representation learning with contrastive predictive coding. *arXiv preprint arXiv:1807.03748*, 2018. 5
- [54] Fernando Paolo, Tsu-ting Tim Lin, Ritwik Gupta, Bryce Goodman, Nirav Patel, Daniel Kuster, David Kroodsma, and Jared Dunnmon. xview3-sar: Detecting dark fishing activity using synthetic aperture radar imagery. *Advances in Neural Information Processing Systems*, 2022. 1
- [55] Gustavo Perez, Subhransu Maji, and Daniel Sheldon. Discount: counting in large image collections with detector-based importance sampling. In *Proceedings of the AAAI Conference on Artificial Intelligence*, pages 22294–22302, 2024. 1
- [56] Lukas Picek, Christophe Botella, Maximilien Servajean, César Leblanc, Rémi Palard, Théo Larcher, Benjamin Deneu, Diego Marcos, Pierre Bonnet, and Alexis Joly. Geoplant: Spatial plant species prediction dataset. *arXiv preprint arXiv:2408.13928*, 2024. 2
- [57] Alec Radford, Jong Wook Kim, Chris Hallacy, Aditya Ramesh, Gabriel Goh, Sandhini Agarwal, Girish Sastry, Amanda Askell, Pamela Mishkin, Jack Clark, et al. Learning transferable visual models from natural language supervision. In *International conference on machine learning*, pages 8748–8763. PMLR, 2021. 2, 5, 6, 7, 14, 17
- [58] Benjamin Recht, Rebecca Roelofs, Ludwig Schmidt, and Vaishaal Shankar. Do imagenet classifiers generalize to imagenet? In *International conference on machine learning*, pages 5389–5400, 2019. 5, 14, 17
- [59] Srikumar Sastry, Subash Khanal, Aayush Dhakal, Di Huang, and Nathan Jacobs. Birdsat: Cross-view contrastive masked autoencoders for bird species classification and mapping. In *Proceedings of the IEEE/CVF Winter Conference on Applications of Computer Vision*, pages 7136–7145, 2024. 2, 3
- [60] Srikumar Sastry, Subash Khanal, Aayush Dhakal, Adeel Ahmad, and Nathan Jacobs. Taxabind: A unified embedding space for ecological applications. In *Proceedings of the IEEE/CVF Winter Conference on Applications of Computer Vision*, 2025. 2, 3, 5, 6, 7, 14
- [61] Brian L Sullivan, Christopher L Wood, Marshall J Iliff, Rick E Bonney, Daniel Fink, and Steve Kelling. ebird: A citizen-based bird observation network in the biological sciences. *Biological conservation*, 142(10):2282–2292, 2009. 2
- [62] Gencer Sumbul, Marcela Charfuelan, Begüm Demir, and Volker Markl. Bigearthnet: A large-scale benchmark archive for remote sensing image understanding. In *IGARSS 2019-2019 IEEE International Geoscience and Remote Sensing Symposium*, pages 5901–5904. IEEE, 2019. 2, 5, 6, 13, 14, 17
- [63] Wenjuan Sun, Paolo Bocchini, and Brian D Davison. Applications of artificial intelligence for disaster management. *Natural Hazards*, 103(3):2631–2689, 2020. 1
- [64] Mélisande Teng, Amna Elmustafa, Benjamin Akera, Yoshua Bengio, Hager Radi, Hugo Larochelle, and David Rolnick. Satbird: a dataset for bird species distribution modeling using remote sensing and citizen science data. *Advances in Neural Information Processing Systems*, 36, 2023. 3, 5, 7
- [65] Catherine Torres de Almeida, Jéssica Gerente, Jamerson Rodrigo dos Prazeres Campos, Francisco Caruso Gomes Junior, Lucas Antonio Providelo, Guilherme Marchiori, and Xinjian Chen. Canopy height mapping by sentinel 1 and 2 satellite images, airborne lidar data, and machine learning. *Remote Sensing*, 14(16):4112, 2022. 1
- [66] Ruben Van De Kerchove, Daniele Zanaga, Wanda Keersmaecker, Niels Souverijns, Jan Wevers, Carsten Brockmann, Alex Grosu, Audrey Paccini, Oliver Cartus, Maurizio Santoro, et al. Esa worldcover: Global land cover mapping at 10 m resolution for 2020 based on sentinel-1 and 2 data. In *AGU Fall Meeting Abstracts*, pages GC45I–0915, 2021. 2
- [67] Grant Van Horn, Oisín Mac Aodha, Yang Song, Yin Cui, Chen Sun, Alex Shepard, Hartwig Adam, Pietro Perona, and Serge Belongie. The inaturalist species classification and detection dataset. In *Proceedings of the IEEE conference on computer vision and pattern recognition*, pages 8769–8778, 2018. 4
- [68] Vicente Vivanco Cepeda, Gaurav Kumar Nayak, and Mubarak Shah. Geoclip: Clip-inspired alignment between locations and images for effective worldwide geolocalization. *Advances in Neural Information Processing Systems*, 2024. 2, 3
- [69] Stefan Voigt, Thomas Kemper, Torsten Riedlinger, Ralph Kiefl, Klaas Scholte, and Harald Mehl. Satellite image analysis for disaster and crisis-management support. *IEEE transactions on geoscience and remote sensing*, 45(6):1520–1528, 2007. 1
- [70] Syed Waqas Zamir, Aditya Arora, Akshita Gupta, Salman Khan, Guolei Sun, Fahad Shahbaz Khan, Fan Zhu, Ling Shao, Gui-Song Xia, and Xiang Bai. isaid: A large-scale dataset for instance segmentation in aerial images. In *Proceedings of the IEEE/CVF Conference on Computer Vision and Pattern Recognition Workshops*, pages 28–37, 2019. 2
- [71] Bingfang Wu, René Gommès, Miao Zhang, Hongwei Zeng, Nana Yan, Wentao Zou, Yang Zheng, Ning Zhang, Sheng Chang, Qiang Xing, et al. Global crop monitoring: a satellite-based hierarchical approach. *Remote Sensing*, 7(4):3907–3933, 2015. 1

- [72] Gui-Song Xia, Jingwen Hu, Fan Hu, Baoguang Shi, Xiang Bai, Yanfei Zhong, Liangpei Zhang, and Xiaoqiang Lu. Aid: A benchmark data set for performance evaluation of aerial scene classification. *IEEE Transactions on Geoscience and Remote Sensing*, 55(7):3965–3981, 2017. [2](#), [5](#), [6](#), [8](#), [13](#), [14](#), [16](#), [17](#)
- [73] Gui-Song Xia, Xiang Bai, Jian Ding, Zhen Zhu, Serge Belongie, Jiebo Luo, Mihai Datcu, Marcello Pelillo, and Liangpei Zhang. Dota: A large-scale dataset for object detection in aerial images. In *Proceedings of the IEEE conference on computer vision and pattern recognition*, pages 3974–3983, 2018. [2](#)
- [74] Yi Yang and Shawn Newsam. Bag-of-visual-words and spatial extensions for land-use classification. In *Proceedings of the 18th SIGSPATIAL international conference on advances in geographic information systems*, pages 270–279, 2010. [5](#), [6](#), [8](#), [13](#), [14](#), [16](#), [17](#)
- [75] Qiangqiang Yuan, Huanfeng Shen, Tongwen Li, Zhiwei Li, Shuwen Li, Yun Jiang, Hongzhang Xu, Weiwei Tan, Qianqian Yang, Jiwen Wang, et al. Deep learning in environmental remote sensing: Achievements and challenges. *Remote sensing of Environment*, 241:111716, 2020. [1](#)
- [76] Zhuo Zheng, Stefano Ermon, Dongjun Kim, Liangpei Zhang, and Yanfei Zhong. Changen2: Multi-temporal remote sensing generative change foundation model. *IEEE Transactions on Pattern Analysis and Machine Intelligence*, 2024. [2](#)
- [77] Xiao Xiang Zhu, Devis Tuia, Lichao Mou, Gui-Song Xia, Liangpei Zhang, Feng Xu, and Friedrich Fraundorfer. Deep learning in remote sensing: A comprehensive review and list of resources. *Geoscience and remote sensing magazine*, 5(4):8–36, 2017. [1](#)
- [78] Xiao Xiang Zhu, Jingliang Hu, Chunping Qiu, Yilei Shi, Jian Kang, Lichao Mou, Hossein Bagheri, Matthias Haberle, Yuansheng Hua, Rong Huang, et al. So2sat lc42: A benchmark data set for the classification of global local climate zones [software and data sets]. *IEEE Geoscience and Remote Sensing Magazine*, 8(3):76–89, 2020. [5](#), [6](#), [8](#), [13](#), [14](#), [15](#), [16](#), [17](#)

WildSAT: Learning Satellite Image Representations from Wildlife Observations

Supplementary Material

A. Datasets

A.1. Training Data Distribution

Figure A1 shows the spatial distribution of all data we collected across the globe. Most of the data are from United States and Europe, corresponding to the wildlife observation data available from citizen science platforms [1, 2].

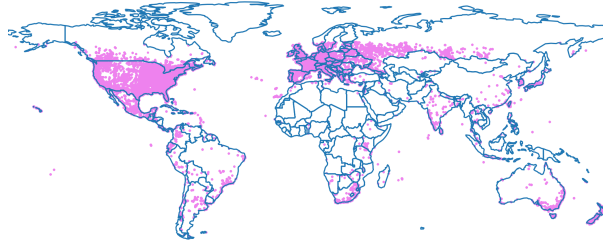


Figure A1. **Distribution of data points with satellite image, environmental covariates, and text.** The alignment of different modalities is guided by the geographic distribution of species.

A.2. Satellite Image Classification Evaluation Datasets

Below we briefly describe the different satellite image classification datasets used for evaluation.

UCM [74] contains 21 classes with 100 each covering USA. Each image is 256×256 with a resolution of 1 ft.

AID [72] contains 30 class, each containing from 220 to 400 images from Google Earth. Each image is 600×600 with a resolution ranging from 0.5 to 8 m.

RESISC45 [7] contains 45 classes with 700 images each, sourced from Google Earth. An image is 256×256 with a resolution ranging from 0.2 to 30 m.

FMoW [8] contains 63 classes from over 200 countries with a total of over 400k images from QuickBird, GeoEye, and WorldView satellites. Images vary in size and resolution and each class has a different number of images.

EuroSAT [27] contains 10 classes of land use and land cover from Europe. Each image is 64×64 with 10 m resolution. The dataset has 27k images with each class having a different number of images.

So2Sat20k [78] contains 17 classes across different climate zones with global coverage. The full dataset contains 400k pairs of Sentinel-1 and Sentinel-2 images. We use the GEO-Bench [37] version referred to as “So2Sat20k” which contains 20k training samples.

BigEarthNet20k (BEN20k) [62] is a multi-label classification dataset with 43 classes. The full dataset is from 10 countries in Europe with 590k Sentinel-2 images. We use the GEO-Bench [37] version “BEN20k” which contains 20k training samples.

B. Additional Implementation Details

WildSAT Training Details. We train each base model on the WildSAT framework for 25 epochs using an Adam optimizer with a learning rate of 1×10^{-4} , with an embedding dimension $d = 512$, and a batch size of 64. Each satellite image is paired with a wildlife observation location. For each of these pairs, a section of text is randomly sampled from the Wikipedia [3] page of the species. A satellite image of the same location, but from a different time, is also randomly sampled for image augmentation. Random cropping, resizing, jitter, and channel mixing are applied as augmentations.

Satellite Image Filtering. All satellite images are from Sentinel-2A and Sentinel-2B. We follow the same data collection procedure from SatlasPretrain [4], where satellite images are downloaded from EU’s Sentinel Data [17]. Each image is 512×512 pixels with a 10 m resolution per pixel. Only images that are tagged with significantly less cloud cover from [4] are used. In addition, we only use satellite images that were taken in the same time range as the wildlife observation data (from 2017 to 2021). This is done since we do not use the exact observation date and time as an input to the model; we consider all observations throughout the time range. At the same time, the text descriptions we use also refer to all types of habitats regardless of time of year.

Encoder	UCM		AID		RESISC45		FMoW		EuroSAT		So2Sat20k		BEN20k	
	[74]		[72]		[7]		[8]		[27]		[78]		[62]	
	Base	+WS	Base	+WS	Base	+WS	Base	+WS	Base	+WS	Base	+WS	Base	+WS
ResNet50 ImageNet1K V2 [58]	94.2	93.6	87.8	86.7	90.5	90.1	47.3	46.0	95.5	96.0	36.1	46.6	55.8	57.5
ResNet50 ImageNet1K V1 [13]	92.5	93.5	90.4	88.8	85.1	84.7	40.7	37.0	88.0	94.9	38.8	48.2	46.7	53.7
ViT-L/16 SatMAE [12]	23.8	86.1	25.1	70.6	26.1	74.6	13.9	33.4	48.3	94.5	15.6	48.6	18.4	51.0

Table A1. **Additional linear probing results on satellite image classification datasets.** Accuracy is reported for all datasets except BEN20k that reports micro F1 score. ‘Base’ refers to the original models specified as the encoder and ‘+WS’ refers to the same models further trained with WildSAT. Consistent with results thus far, fine-tuning models with species observation generally show significant improvement over the base models.

	UCM	AID	RESISC45	FMoW	EuroSAT	So2Sat20k	BEN20k
	[74]	[72]	[7]	[8]	[27]	[78]	[62]
TaxaBind [60]	80.5	67.7	72.6	31.2	85.2	33.9	47.6
GRAFT [45]	81.1	76.1	83.3	39.3	90.9	36.6	48.0
CLIP [57]	94.5	86.3	92.1	51.5	92.2	37.6	47.1
WildSAT (Ours)	96.3	88.0	93.0	52.8	97.1	49.7	59.1

Table A2. **Linear probing results on downstream satellite classification datasets using models with CLIP as the base.** Results are reported as accuracy, except for BEN20k which uses micro F1. TaxaBind and GRAFT both fine-tune a CLIP backbone and use additional modalities such as text, ground images, and satellite images for cross-modal tasks. WildSAT outperforms both the standard CLIP and the previous methods that also fine-tune on CLIP.

Multi-spectral Baselines. Prithvi-100M [31] and SatCLIP [34] originally use multi-spectral data in their pre-training. However, for general applicability and easy comparisons with other models, we only use RGB bands. When WildSAT is applied to these models, we only fine-tune with the three bands, and set other bands to zero. At the same time, when applying both the base models and WildSAT fine-tuned models on downstream satellite image datasets, we also set other bands to zero.

C. Additional Results

C.1. Satellite Image Classification

ImageNet V1 Results. Table A1 shows results on the ImageNet V1 base model that previous works have used [44, 46]. The results in Table 1 in the main paper include a base model using ImageNet V2 (also included in Table A1 for reference) which has generally better performance across the downstream satellite image datasets. Table A1 additionally shows results on SatMAE [12], a ViT-L/16 model that was pre-trained with the MAE framework on satellite images. Similar to previous results, WildSAT improves performance across the seven satellite image classification datasets evaluated.

WildSAT outperforms CLIP-based models. Table A2 displays the result for each evaluation dataset across different CLIP-based models. All models in the table starts with a pre-trained CLIP ViT-B/16 model [57]. TaxaBind[60] and GRAFT [45] use additional modalities such as ground images, text, and audio to improve model performance on cross-modal tasks such as zero-shot image-text retrieval. However, we show that while these same models do well on zero-shot tasks, they tend to “forget” some of the original image representations, with linear probing performance on downstream datasets lower than that of the original CLIP model. With WildSAT applied to CLIP, we show that we can outperform not only other CLIP-based models, *i.e.* GRAFT and TaxaBind, but also outperform the standard CLIP model across all the datasets in the evaluation. We hypothesize we can prevent “forgetting” by applying parameter efficient fine-tuning on out-of-domain pre-trained models such as CLIP. We further show this in Table A5.

WildSAT reduces errors on habitat-related classes. Figure A2 shows the confusion matrix of a sample result on the So2Sat20k test set. The matrix on the left shows the result of a base ImageNet pre-trained model, and the right matrix shows the result when WildSAT is applied. We show that WildSAT improvements on the true positive counts along the diagonal are largely due to fewer false positives on habitat-related classes. Looking at the second row of both matrices (class ‘Sparsely built’), the true positive count doubled from 24 to 48. A lot of this improvement comes from less false positives on ‘Scattered

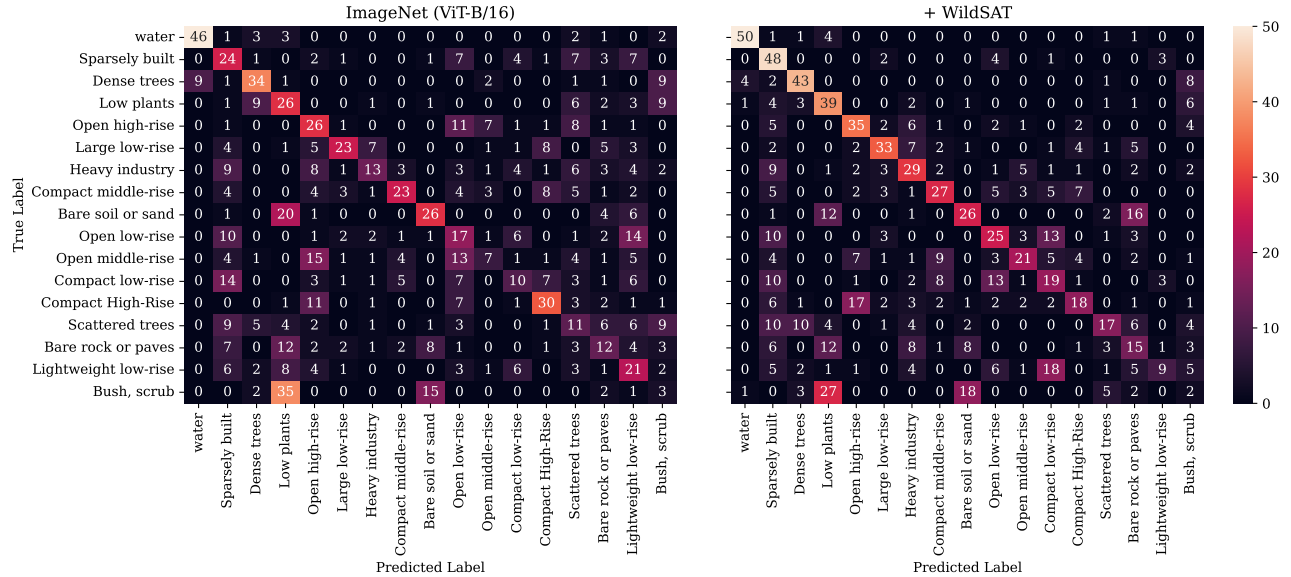


Figure A2. Confusion matrices comparing the predictions of an ImageNet base model and a WildSAT fine-tuned model on the So2Sat20k dataset [78]. Both models use a ViT-B/16 architecture. Each matrix displays the result on the provided So2Sat20k test set in GEO-Bench [37].

trees’ (from 7 false positives to 0), ‘Bare rock or paves’ (from 3 false positives to 0), and ‘Dense trees’ (from 1 false positive to 0)—all of which are habitat-related attributes. Similar trends can be observed on other classes as well such as in ‘Dense Trees’ and ‘Low Plants’ where we see higher true positive counts with WildSAT.

C.2. Additional Ablations

WildSAT improves models by covering model-specific gaps. Table A3 displays an ablation study conducted on two different types of models: a ResNet50 SeCo [46] model and a ViT-B/16 ImageNet [13] model. SeCo is pre-trained with a contrastive objective on time augmented satellite images (*i.e.* satellite images from the same location, but from different seasons). This objective is similar to the \mathcal{L}_{img} term (Eqn. 1 in the main paper) in the loss function of our WildSAT framework. Thus, we see from Table A3, that simply adding the image augmentation term (‘img-a’) only slightly improves the average performance across the downstream datasets (from 70.1% to 71.8%). This small improvement could be attributed to the additional examples related to habitats that are possibly not as well-represented in the SeCo dataset. However, if we add other modalities such as text and location (in addition to the satellite image augmentation), we see a larger improvement with an average performance of 74.2% and 75.2%, respectively. In contrast, an ImageNet pre-trained model benefits from satellite image augmentations (\mathcal{L}_{img} or ‘img-a’) since it was trained on a different domain. Simply adding the image augmentation term improved average performance from 76.9% to 82.3%. Further adding other modalities such as text and location also pushes the performance higher to 83.6%. These results support our hypothesis that WildSAT can complement and further improve different architectures by leveraging the different modalities.

Location encoder ablation. Table A4 shows an ablation study conducted on our choice of the location encoder. We use a ResNet50 SeCo encoder as the base model, and report accuracy on downstream classification datasets. All rows in the table use WildSAT with satellite images and text ($\mathcal{L}_{\text{img}} + \mathcal{L}_{\text{txt}}$), which are matched based on the location—*i.e.* location is implicitly used in all the results, and we ablate which encoder to use for explicitly including location as an input. We replace the location encoder in our WildSAT framework with one of the following: no model (*i.e.* use the position encoded latitude and longitude and/or the raw environmental covariates vector), SatCLIP [34], or SINR [11]. We use the SatCLIP pre-trained location encoder that takes the latitude and longitude as an input. For SINR, we explore the two variants of using (1) just the location (‘loc’) or (2) both the location (‘loc’) and environmental covariates (‘env’). We find that the best average performance uses SINR with both the location and environmental covariates.

ResNet50 SeCo [46]									
Loss Terms	loc	env	text	img-a	UCM [74]	AID [72]	RESISC45 [7]	So2Sat20k [78]	Average
Base Model					86.1%	74.3%	80.2%	39.9%	70.1%
\mathcal{L}_{loc}	✓				84.0%	76.2%	81.1%	43.5%	71.2%
\mathcal{L}_{loc}	✓	✓			84.1%	76.3%	83.0%	38.7%	70.5%
\mathcal{L}_{txt}			✓		82.8%	74.4%	79.6%	39.5%	69.1%
$\mathcal{L}_{txt} + \mathcal{L}_{loc}$	✓		✓		84.3%	72.7%	78.5%	41.3%	69.2%
$\mathcal{L}_{txt} + \mathcal{L}_{loc}$	✓	✓	✓		84.0%	75.8%	81.8%	40.0%	70.4%
\mathcal{L}_{img}				✓	83.3%	75.0%	82.9%	46.0%	71.8%
$\mathcal{L}_{img} + \mathcal{L}_{loc}$	✓			✓	85.7%	77.9%	86.7%	46.2%	74.2%
$\mathcal{L}_{img} + \mathcal{L}_{loc}$	✓	✓		✓	85.3%	77.1%	85.7%	48.2%	74.0%
$\mathcal{L}_{img} + \mathcal{L}_{txt}$			✓	✓	86.6%	77.0%	84.7%	48.6%	74.2%
$\mathcal{L}_{img} + \mathcal{L}_{txt} + \mathcal{L}_{loc}$	✓		✓	✓	86.8%	78.1%	86.0%	49.0%	75.0%
$\mathcal{L}_{img} + \mathcal{L}_{txt} + \mathcal{L}_{loc}$	✓	✓	✓	✓	88.8%	79.6%	86.3%	46.0%	75.2%

ViT-B/16 ImageNet [13]									
Loss Terms	loc	env	text	img-a	UCM [74]	AID [72]	RESISC45 [7]	So2Sat20k [78]	Average
Base Model					93.2%	84.4%	88.2%	41.8%	76.9%
\mathcal{L}_{loc}	✓				95.2%	85.8%	89.3%	43.4%	78.4%
\mathcal{L}_{loc}	✓	✓			94.7%	86.2%	88.8%	44.2%	78.5%
\mathcal{L}_{txt}			✓		96.1%	85.1%	88.9%	42.2%	78.1%
$\mathcal{L}_{txt} + \mathcal{L}_{loc}$	✓		✓		95.6%	86.5%	89.6%	39.6%	77.8%
$\mathcal{L}_{txt} + \mathcal{L}_{loc}$	✓	✓	✓		95.1%	86.2%	89.7%	45.0%	79.0%
\mathcal{L}_{img}				✓	97.1%	87.1%	91.5%	53.7%	82.3%
$\mathcal{L}_{img} + \mathcal{L}_{loc}$	✓			✓	97.1%	88.1%	91.7%	54.0%	82.7%
$\mathcal{L}_{img} + \mathcal{L}_{loc}$	✓	✓		✓	96.8%	88.6%	92.1%	52.7%	82.6%
$\mathcal{L}_{img} + \mathcal{L}_{txt}$			✓	✓	96.9%	87.7%	92.0%	54.3%	82.7%
$\mathcal{L}_{img} + \mathcal{L}_{txt} + \mathcal{L}_{loc}$	✓		✓	✓	97.1%	87.9%	91.9%	53.4%	82.6%
$\mathcal{L}_{img} + \mathcal{L}_{txt} + \mathcal{L}_{loc}$	✓	✓	✓	✓	97.5%	88.9%	93.0%	55.2%	83.6%

Table A3. **Ablation of the various components of the WildSAT framework.** We ablate on SeCo [46], a self-supervised pre-training method that applies contrastive learning on seasonal augmentations of images, and on ImageNet [13], a supervised pre-training on ImageNet. Through the different modalities in WildSAT, we can improve model-specific gaps.

ResNet50 SeCo [46]									
No Model	SatCLIP	SINR	UCM	AID	RESISC45	So2Sat20k	Average		
loc	env	loc	loc	env	[74]	[72]	[7]	[78]	
					86.6%	77.0%	84.7%	48.6%	74.2%
✓					87.3%	78.1%	85.5%	48.3%	74.8%
✓	✓				86.3%	76.3%	84.9%	47.2%	73.7%
✓	✓				87.0%	77.4%	85.1%	48.4%	74.5%
		✓			86.0%	78.2%	85.5%	50.0%	74.9%
			✓		86.8%	78.1%	86.0%	49.0%	75.0%
			✓	✓	88.8%	79.6%	86.3%	46.0%	75.2%

Table A4. **Ablation of the location encoder.** These runs assume both the text (\mathcal{L}_{txt}) and the image augmentation (\mathcal{L}_{img}) are already part of the model, which implicitly uses location (since images and text are matched based on location). We ablate the explicit addition of location as an input through different location encoders. We explore using no model (*i.e.* directly just using the latitude/longitude or environmental covariates), SatCLIP [34], and SINR [11]. The last row of the table corresponds to our WildSAT setup.

Encoder		PEFT	UCM [74]	AID [72]	RESISC45 [7]	FMoW [8]	EuroSAT [27]	So2Sat20k [78]	BEN20k [62]
ResNet50	ImageNet1K [58]		91.3%	82.0%	85.6%	42.1%	95.0%	47.0%	56.1%
ResNet50	ImageNet1K [58]	✓	93.6%	86.7%	90.1%	46.0%	96.0%	46.6%	57.5%
ViT-B/16	CLIP [57]		82.1%	71.0%	75.3%	34.9%	93.4%	50.4%	49.0%
ViT-B/16	CLIP [57]	✓	96.3%	88.0%	93.0%	53.6%	97.1%	49.7%	59.1%
ResNet50	SatlasNet [4]		90.1%	79.4%	85.4%	42.4%	95.4%	44.8%	56.4%
ResNet50	SatlasNet [4]	✓	86.9%	76.8%	82.0%	35.7%	94.1%	41.6%	51.6%
ResNet50	SeCo [46]		88.8%	79.6%	86.3%	42.8%	95.5%	46.0%	57.3%
ResNet50	SeCo [46]	✓	86.7%	77.3%	83.2%	37.3%	94.0%	44.4%	54.8%

Table A5. **Ablation of parameter efficient fine-tuning (PEFT) when applied with WildSAT.** Models pre-trained on out-of-domain datasets (*e.g.* ImageNet, CLIP) that are fine-tuned with PEFT can perform better on downstream tasks by preserving original representations from the base model. In contrast, models pre-trained on in-domain datasets (*e.g.* SatlasNet, SeCo) show limited improvement from PEFT since the fine-tuning is in the same domain as the pre-training (*i.e.* satellite images)—fine-tuning all layers has better performance.

Parameter efficient fine-tuning (PEFT) preserves out-of-domain pre-training representations. Table A5 displays the effect of fine-tuning all parameters of a given base model compared to fine-tuning specific layers (*i.e.* applying PEFT). We compare the effect on out-of-domain pre-trained models (*e.g.* ImageNet [58], CLIP [57]), and in-domain pre-trained models (*e.g.* SatlasNet [4], SeCo [46]). We find that out-of-domain pre-trained models have better downstream performance by applying scale and shift fine-tuning [20, 39], or by applying DoRa [47]. By fine-tuning specific layers, the models retain some of the original representations learned from the pre-training (*i.e.* ImageNet or CLIP) so that performance does not deteriorate compared to the base models. This has a significant impact on large models such as ViT, since fine-tuning all weights alters many parameters and risks shifting them in suboptimal directions. On the other hand, while applying PEFT for in-domain pre-trained models SatlasNet [4] and SeCo [46] improves performance compared to the base model, we see better performance when directly fine-tuning all the layers. This may be because the model has already undergone pre-training on satellite images, making additional pre-training on similar data from WildSAT result in a non-disruptive shift.

C.3. Zero-shot Retrieval

In Figure A3, we display more zero-shot retrieval examples. The first row of examples demonstrates retrieval of general landscapes such as ‘rainforest’ or ‘mountains’. The second row demonstrates retrieval of wildlife habitats. We enumerate each of the wildlife examples below including their expected habitats. All the enumerated habitats are consistent with the retrieved satellite images.

Description of the wildlife examples from the second set of rows in Figure A3:

1. ‘house sparrow’ is a small, common bird typically found in urban areas.
2. ‘albatross’ is a large bird commonly found in the sea.
3. ‘sandpiper’ is a small bird that dwells in the coast.
4. ‘horned lark’ is a bird species found in open land such as on farmland, on prairies, and in deserts.
5. ‘cactus’ is a type of plant commonly found in the desert.
6. ‘rock pigeon’ is a bird commonly found in urban and residential areas.
7. ‘virginia rail’ is a bird found in freshwater and brackish marshes, and sometimes salt marshes in winter.
8. ‘american marten’ is a North American mammal that is found in forests, and broadly distributed in North America from Alaska and Canada to New York.

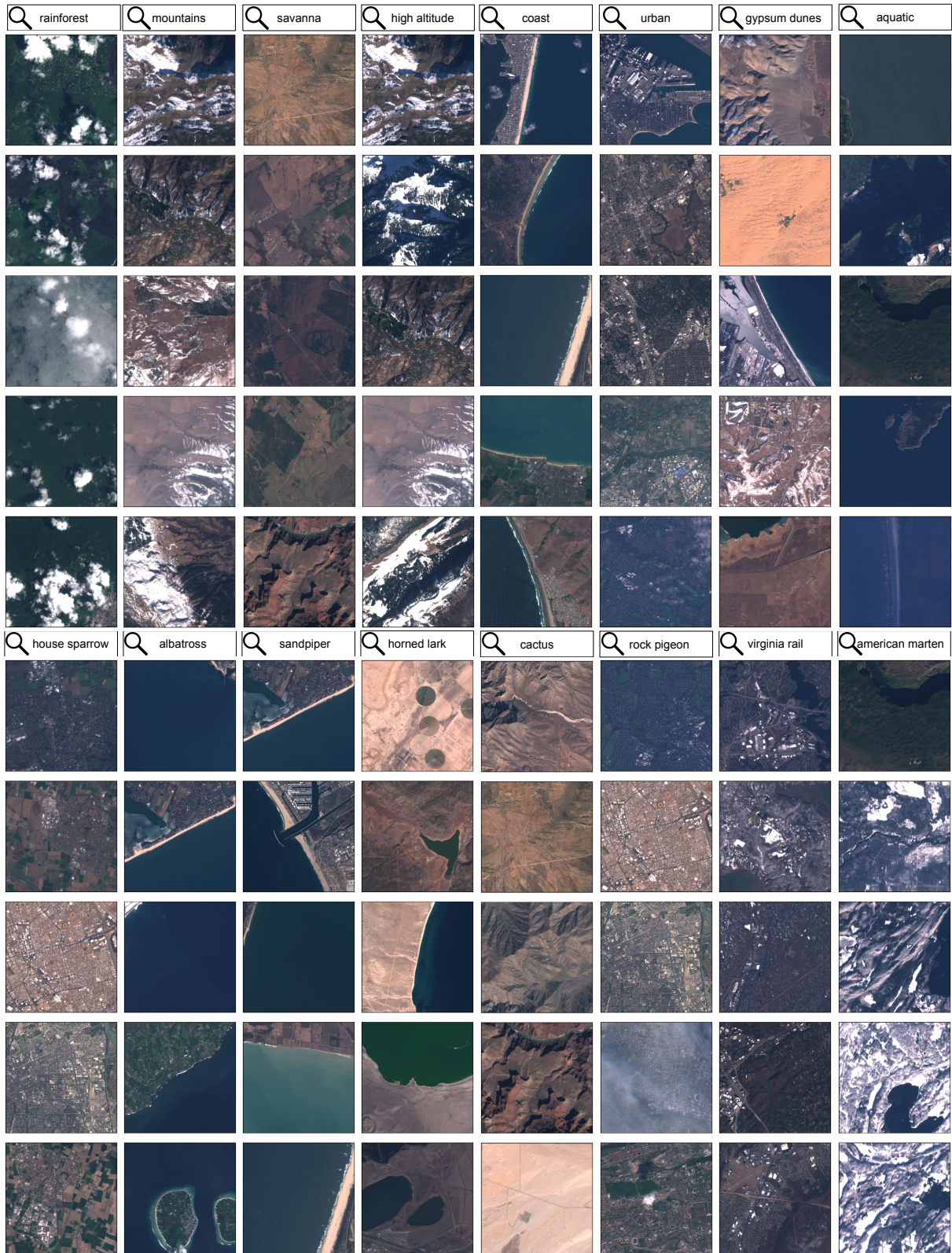


Figure A3. Additional zero-shot results for text-based satellite image retrieval.